Scripta Materialia 194 (2021) 113668

Contents lists available at ScienceDirect

Scripta Materialia

journal homepage: www.elsevier.com/locate/scriptamat

Entropy-induced transition on grain-boundary migration in multi-principal element alloys

Fusheng Tan[a], Jia Li[a], Hui Feng[a], Qihong Fang[a,*], Chao Jiang[a,*], Yong Liu[b,*], Peter K Liaw[c]

[a] State Key Laboratory of Advanced Design and Manufacturing for Vehicle Body, Hunan University, Changsha 410082, PR China
[b] State Key Laboratory of Powder Metallurgy, Central South University, Changsha 410083, PR China
[c] Department of Materials Science and Engineering, The University of Tennessee, Knoxville, TN 37996, USA

ARTICLE INFO

Article history:
Received 27 September 2020
Revised 28 November 2020
Accepted 8 December 2020
Available online 21 December 2020

Keywords:
Grain boundary
Multi-principal element alloy
Grain boundary migration

ABSTRACT

In-depth understanding of grain boundaries (GBs) in multi-principal element alloys (MPEAs) is considered significant for designing MPEAs by GB engineering. This work explores the nanoscale GB structure and migration mechanism in MPEAs using atomic simulations. The GB-roughening transformation is observed as the mixing entropy increases, and the effect of entropy is confirmed by thermodynamic analysis. The entropy-induced transition of GB migration is proved: 1) the "concentrated shuffling mechanism" controls the migration of ordered GBs in low-entropy systems, leading to the obviously stepwise migration; 2) the "dispersed shuffling mechanism" dominates the migration of disordered GBs in high-entropy systems, resulting in the continuous migration manner.

The grain boundary (GB) movements, such as GB sliding and migration, play an important role in the microstructure evolution and macroscale property of materials [1,2]. To date, lots of researchers have been devoted to understanding the mechanism of the GB migration (GBM) [3–7]. Several mechanisms have been proposed, such as the shuffling mechanism [6], the disconnection-mediated mechanism [4] and the secondary-GB-dislocations-step mechanism [7]. For instance, in-situ transmission electron microscopy experiments show that the stress-induced GBMs and capillary-induced GBMs in Au films are controlled by the secondary-GB-dislocations-step mechanism and the shuffling mechanism, respectively [6,7]. A recent experiment shows that the shear-coupled GBM in bicrystal Au is realized by the disconnection-mediated mechanism [4]. Most of the migration mechanisms proposed so far are based on the studies of traditional metallic materials, which usually contain only one principal element.

In sharp contrast to traditional alloys, the multi-principal element alloys (MPEAs) comprise several elements mixed in an equal or near-equal atomic fraction. MPEAs attract extensive research interest in the field of engineering materials due to their outstanding mechanical properties [8,9], which attribute to their unique characteristics, such as the concentration waves [10] and chemical short-range order (SRO) [11]. These characteristics also have a great influence on the microstructures [12–14]. Recent research activities suggest that GBs in $Ni_{43.9}Co_{22.4}Fe_{8.8}Al_{10.7}Ti_{11.7}B_{2.5}$ and CuNiCoFe MPEAs exhibit complex structures and motion patterns [12,13], which are hardly detected in conventional alloys. Up to now, the motion of GBs in MPEAs is still studied rarely. Motivated by this, the present study addresses the GB structure and migration mechanism in MPEAs with different mixing entropies. Using atomic simulations (Section 1 in Supplemental Materials), the disordered GBs and changed migration mechanisms are observed in high-entropy MPEAs. Thermodynamics analysis further confirms the effect of mixing entropy on the GB morphology.

Following the Boltzmann's hypothesis, the mixing entropy, ΔS_{mix}, of an N-element equimolar alloy changing from an elemental to a random-solution state can be calculated from $\Delta S_{mix} = R \ln N$, where R is the gas constant. Accordingly, the metal/binary, ternary, and quaternary/quinary samples are respectively classified as low-, medium-, and high-entropy systems. Here, it should be note that the term "mixing entropy" used in this paper refers to the mixing configurational entropy of the global system produced by mixing multiple elements. The considered entropy change refers to the change in the entropy of one-element system ($\Delta S_{mix} = 0 \times R$) to five-principal system ($\Delta S_{mix} = 1.61 \times R$). Because the element distributions in the bulk and GB are identical, the mixing entropy between GB and the entire system have negligible differences.

The atomic configurations of the GB in different samples are shown in Figs. 1 and 2. To describe the static and dynamic GB structures, both GBs before and during migration are displayed. Similar to the previous work [3], the static low-entropy sample

* Corresponding authors.
E-mail addresses: fangqh1327@hnu.edu.cn (Q. Fang), jiangc@hnu.edu.cn (C. Jiang), yongliu@csu.edu.cn (Y. Liu).

https://doi.org/10.1016/j.scriptamat.2020.113668
1359-6462/

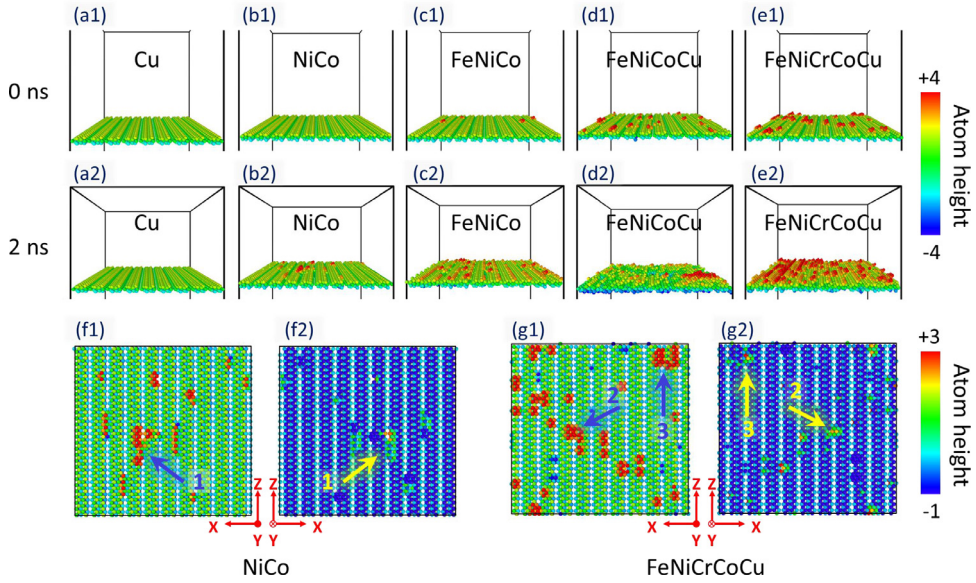

Fig. 1. (a–e). Snapshots of the GB structure before (0ns) and during (2ns) migration, showing the degree of GB roughness. (f and g) Atomic details of GB planes of NiCo (2ns) and FeNiCrCoCu (0ns) samples, showing the details of a rough GB. The blue arrows mark the convex parts of the GB plane, while the yellow arrows mark the corresponding concave parts of the same plane. All atoms are colored according to their heights relative to the average GB position. (For interpretation of the references to color in this figure legend, the reader is referred to the web version of this article.).

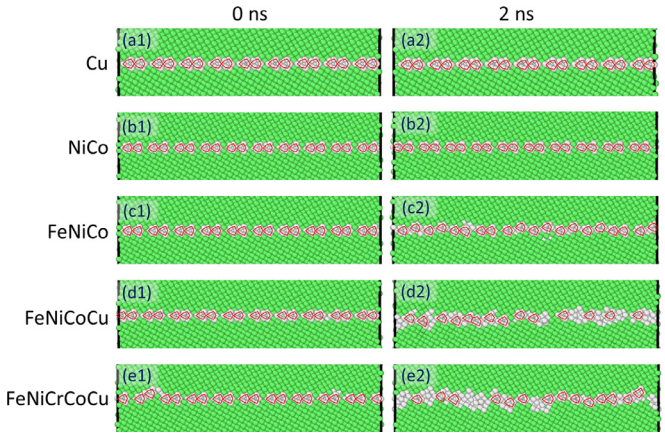

Fig. 2. Magnification of the GB structures in different samples before (0 ns, a1–e1) and during (2 ns, a2–e2) migration. Established GB structure units are indicated by red lines. The atoms are colored according to the common neighbor analysis parameter: green are FCC atoms and white are unknown atoms. (For interpretation of the references to color in this figure legend, the reader is referred to the web version of this article.).

exhibits a smooth GB structure (Fig. 1(a1–b1)) with repeating structure units (Fig. 2(a1–b1)). Although similar kite-shaped structure units are also observed in static medium- and high-entropy MPEAs (Fig. 2(c1–e1)), GB planes of these samples are rough (Fig. 1(c1–e1)): some segregation-like atom groups appear on GB planes. A similar configurational change of microstructure in MPEAs is also observed in the previous literature [14]. Looking closely at these GB planes, it can be found that each convex part of these GB planes corresponds to a concave part of the same position on the back of the GB (Fig. 1(f and g)). This means that the morphologies of these GBs have indeed changed, rather than simply absorbing atoms to GBs. This trend may be connected to SRO or concentration waves (Supplemental Fig. S5), which influence the local stress field [15], and then affects GB structures.

For the static GBs presented in Fig. 2(a1–e1), the kite-shaped units are obvious, and the structure units for all samples are identical. But for dynamic cases, both the morphologies and characteristic structure units of GBs change greatly with the entropy, which can be obviously observed from Fig. 1(a2) to (e2). The quantitative results of GB roughness further confirm that the GBs in high-entropy samples are rougher than those in low- and medium-entropy samples (Supplemental Fig. S6). The GB structure units are no longer identical for all MPEA samples (Fig. 2(a2–e2)). On one hand, the shapes of some structure units are distorted, especially in high-entropy samples. Other structure units are totally disordered, and thereby cannot be outlined by lines. This feature is a direct evidence of the structural change of GBs. On the other hand, these structure units are not in the same Y coordinate, which directly influences the morphology of GB planes.

Compared to the GBs that are composed of regularly arranged structural units in low-entropy samples, the GBs in medium- and high-entropy samples are obviously more chaotic, as evidenced by the distorted or even disordered structural units (Fig. 2(a2–e2)). In other words, the GBs in low-entropy samples are smooth/ordered, while the GBs in medium/high-entropy systems are rough/disordered. These findings indicate a mixing entropy-induced GB roughening transformation, since mixing entropy is one of the most intuitive thermodynamic state variables caused by multiple elements mixing. From a deeper perspective, the random distribution of different elements should be the root cause of the GB roughening. In this case, it is reasonable to attribute the GB roughening transformation to atomic-scale concentration waves or SRO [10,11]. However, both concentration waves and SRO are hard to be accurately quantified, which makes it difficult to distinguish the studied samples based on them. More importantly, the mixing entropy is adequate to describe the random distribution of different elements, which is exactly the underlying reason of both concentration waves and SRO. The role of entropy on the GB roughening will be further verified by a subsequent thermodynamic analysis.

Similar GB structural transformation has been observed in both simulations and experiments (Section 3 in Supplemental Materials). According to previous studies [16,17], the roughening transition occurs when the temperature rises to the roughening temperature. In these systems, an increase in temperature

always accompanies by an increase in thermal entropy. So, it is hard to distinguish the role of temperature and entropy. Other research shows that the GB with a low relative solute excess remains ordered until it reaches a high global impurity element concentration, and then abruptly transforms into a disordered GB [18,19]. Combining these studies, the present work suggests that the entropy may be the underlying physical mechanism for the GB transformation from the order state in low-entropy systems to disordered state in high-entropy systems.

In order to further confirm the effect of mixing entropy on GB roughening, the thermodynamic stability of the rough GB in MPEA systems is discussed (Section 4 in Supplemental Materials). The interface between the GB and bulk phases can be regarded as being composed of many small interface pieces (Supplemental Fig. S2(a)). Consider one representative interface piece sandwiched between the GB and bulk phases (Supplemental Fig. S2(b)). The free energy, ΔF_{rough}, due to the convexity of the rough boundary can be estimated as:

$$\begin{aligned}\Delta F_{rough} &\approx \Delta H_{rough} - T\Delta S_{rough} \\ &= N^* k_B T(\alpha C_A C_B + C_A \ln C_A + C_B \ln C_B)\end{aligned} \tag{1}$$

where α is a quantity related to the binding energy of atom pairs, A-A, B-B, and A-B. The dependence of the free energy, ΔF_{rough}, on the concentration, C_A, shows that, when $\alpha \leq 2$, ΔF_{rough} is minimized at $C_A = 50\%$ (Supplemental Fig. S2(a)). It indicates that the rough interface is stable, when elements A and B atoms are equimolar. The value of α can be estimated as [20]:

$$\alpha \approx \left(\frac{\delta^*}{\delta}\right)\frac{\Delta H_m}{RT_m} \tag{2}$$

where $\Delta H_m \approx RT$ is the latent heat of melting for metallic materials [20]. For FCC alloys, the nearest neighbor, δ, for each atom is 12, and the maximum value of δ^* is 24 (the number of the third neighbor atoms in a FCC lattice). Therefore, α is always smaller than 2 for FCC alloys. It represents that the rough interface pieces in an equimolar A-B system is thermodynamically stable. Furthermore, the present theoretical model verifies that the rough interface is due to the mixing of equimolar atoms. Therefore, for any given interface, the possibility of roughness increases with the component numbers of an equimolar atomic system. This finding is consistent with the simulation results, i.e., GB roughness is highest in high-entropy samples.

Fig. 3 displays the change of the GB position with the simulation time. Note that the GB migration is driven by the mechanical shearing and the shrink-wrapped boundary condition is applied in Y direction (Section 1 in Supplemental Materials). For the pure metal sample in Fig. 3(a), the entire stick-slip GBM event is repeated for the duration of the simulation. Such a regular stepwise migration is also observed in other pure metals, such as aluminium [21]. However, the state of the GBM in MPEA samples changes greatly (Fig. 3(b–e)). The stick-slip characteristic for the MPEA samples is not obvious, compared with the pure metal. Take the quinary sample in Fig. 3(e) as an example, although the GB still stagnates at some positions for a while (e.g., 0.9ns-1.0ns), the stick-slip behaviour is rarely captured during the whole simulation. Most of the time, the GB in the quinary sample moves continuously. The comparison from Fig. 3(a) to (e) reveals that the frequency of the stick-slip event decreases with the increasing mixing entropy. This finding suggests a possible change in the migration mechanism due to the mixing entropy. Previous research revealed that the rough boundary moves continuously so that its position is linear with time, while the smooth boundary moves in a stepwise manner, characterized by sudden motion events interspersed with static periods of varying durations [16,17]. This phenomenon further verifies a transformation from the smooth GB to rough GB as the mixing entropy increases, which agrees with the result obtained from Figs. 1 and 2.

The atomic-scale mechanisms of the coupled GB motion are determined by examining multiple snapshots stored during the simulations along with the relevant parts of atomic trajectories. Two different types of mechanisms are found, corresponding to the stepwise and continuous GBM. Fig. 4(a) shows the dynamic GBM in a pure copper, where the initial GB with perfect structure units is smooth (Fig. 4(a1)). Under a sufficient strain, one GB-atom group first shuffles locally on the boundary plane (Fig. 4(a2)). This atom group then spreads laterally on the GB plane, raising the position of more parts of the GB (Fig. 4(a3)). Eventually, the shuffling action traverses the whole GB, thus completing a one-step migration of the GB (Fig. 4(a4)). Here, the “one-step migration” represents the movement of a GB from its current position to a new position. This GBM process in the elemental sample is exactly the procedure described by the classic shuffling mechanism [6], which is commonly used to describe the migration of high-angle GBs in traditional metallic materials.

Looking closely at the one-step migration of the quinary sample in Fig. 4(c), another migration mechanism can be found. In contrast with the pure metal, the migration in the quinary sample always begins with a rough GB, as presented in Fig. 4(c1). When the local shear stress around the GB accumulates and increases, the roughness of the GB increases (Fig. 4(c1–c3)). The GB roughening, in fact, is caused by the dispersed shuffling of atoms across the GB, which is enhanced by the increased shear strain. With more atoms shuffling events taking place, the position of a GB gradually increases, and finally realizes the one-step GBM. Essentially, such a migration mechanism can be also viewed as a “shuffling mechanism”.

The main difference between the two migration processes for smooth and rough GBs lies in the formation location of shuffled atom groups. For smooth GBs, atoms shuffle concentratively to form a single atom group, which grows fast, as presented in Fig. 4(a2–a3). However, for rough GBs, many small atom groups are dispersedly and gradually formed on the GB plane. Thus, it is reasonable to name the mechanism that dominates the smooth GB as the “concentrated shuffling mechanism”, and for rough GBs as the “dispersed shuffling mechanism”.

The initial state of the smooth GB is always ordered, so that the atom group is hard to shuffle and the GBM would be stagnant for a while after reaching a new position, as shown in Fig. 3a. Nevertheless, the GB is always rough in MPEAs, which means that there are always some shuffled atoms on the GB plane. Such rough GBs may decrease the shuffling barrier of new atoms groups. In this context, the stagnant GB is hard to capture in Fig. 3e. At the later stage of the one-step migration of rough GBs, the dispersed shuffling may transform into the concentrated shuffling, if enough dispersed small atom groups generate closely and thereby forge into a larger atom group. Then, this process would enhance the one-step GBM. Evidence can be found via comparing the time consumption from Fig. 4(c1) to (c2) and Fig. 4(c3) to (c4), which are 0.08 ns and 0.01 ns, respectively.

Strictly speaking, the GBM in the studied samples is under the control of the competition between the concentrated and dispersed shuffling mechanism, since there are both stepwise and continuous periods included in Fig. 3(b–e). The migrations in the pure-metal sample, and the high-entropy sample are two extreme cases: 1) the former is totally controlled by the “concentrated shuffling mechanism”; 2) the latter is dominated by the “dispersed shuffling mechanism”. The GBM in the binary and ternary samples can be viewed as the combination of that in the pure-metal and high-entropy samples. This conclusion is proven by Fig. 3(b and c), in which both the stepwise and continuous migration events are easily captured.

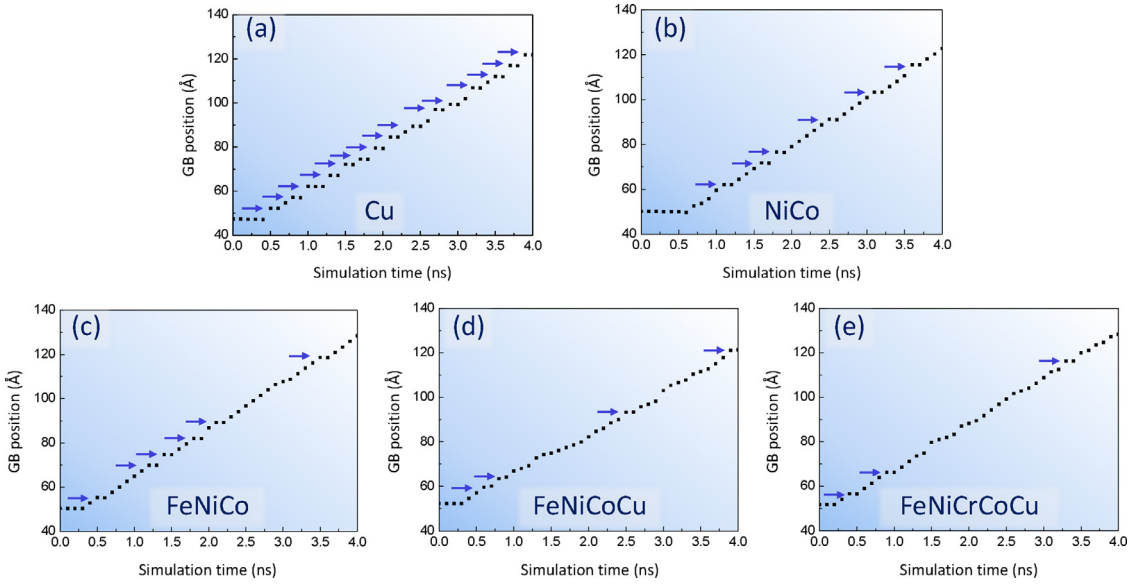

Fig. 3. The GB positions at different moments. The blue arrows mark the "stick-slip" migration events, where the GB position stagnates for a while. (For interpretation of the references to color in this figure legend, the reader is referred to the web version of this article.).

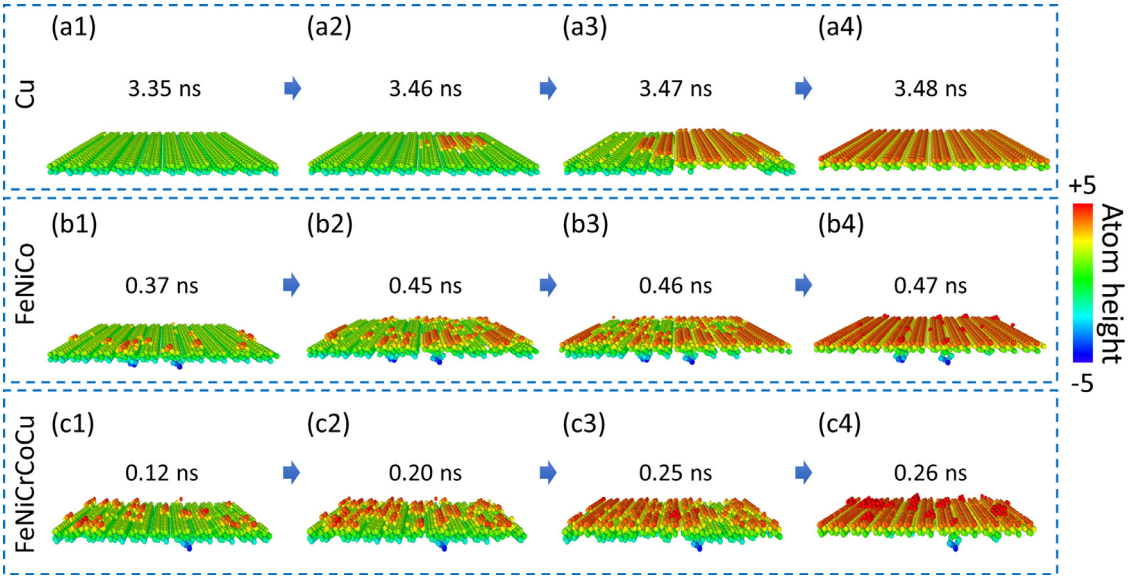

Fig. 4. Details of the one-step GB-migration process for Cu, FeNiCo, and FeNiCrCoCu samples, showing the migration mechanisms for MPEAs with different mixing entropies.

Previous studies suggest that GB roughening always causes a decrease in the migration barrier [16,17]. The functional relation between the entropy and migration barrier is an interesting issue, but it is hard to obtain just based on the present work that has only a small amount of data. The entropy-induced change in GBM barrier will also influence the microstructural evolution and mechanical properties of materials. Logically, the grain growth can be easily activated due to the decrease in the intrinsic migration barrier. However, other factors, like the diffusion ability of specific elements and the presence of SRO, have inevitable effects on the GBM and thereby the grain growth. Comprehensively, how entropy affects the grain growth behaviour in an actual MPEA needs further study. For nanocrystalline MPEAs, the decrease in the GBM barrier may be beneficial to the plastic deformation and the optimization of comprehensive mechanical properties [22,23]. This result provides a new idea for the design of nanocrystalline materials with an excellent strength/toughness balance.

In summary, the structures and migration mechanisms of GBs in MPEAs are studied, using molecular dynamics simulations. The results demonstrate a mixing entropy-induced GB transformation from the smooth/order state in low-entropy systems to rough/disordered state in high-entropy systems. Equilibrium thermodynamics is applied to evaluate the stability of the rough GBs in MPEAs, and it uncovers the close relationship between the GB roughening and mixing entropy. The smooth/ordered GBs in low-entropy samples move in a stepwise manner, while the rough/disordered GBs in high-entropy samples migrate continuously. Combining with the atomic details of GB-migration processes, it reveals that the GB-migration mechanism would change from "concentrated shuffling mechanism" to "dispersed shuffling mechanism" with the increase mixing entropy of systems. These results lay a foundation for theoretically modelling GBs and understanding GB-related phenomenon in MPEAs.

Declaration of Competing Interest

All authors declare that No conflict of interest exists.

Acknowledgement

The authors would like to appreciate the supports from the Foundation for Innovative Research Groups of the National Natural Science Foundation of China (Grant No. 51621004), the National Natural Science Foundation of China (51871092 and 11772122), the State Key Laboratory of Advanced Design and Manufacturing for Vehicle Body (71865015), and the National Key Research and Development Program of China (2016YFB0700300). P.K. Liaw very much appreciates the support from (1) the National Science Foundation (DMR-1611180 and 1809640) with the program directors, Drs. J. Yang, G. Shiflet, and D. Farkas and (2) the U.S. Army Research Office Project (W911NF-13-1-0438 and W911NF-19-2-0049) with the program managers, Drs. M. P. Bakas, S. N. Mathaudhu, and D. M. Stepp.

Supplementary materials

Supplementary material associated with this article can be found, in the online version, at doi:10.1016/j.scriptamat.2020.113668.

References

[1] R.Z. Valiev, Y. Estrin, Z. Horita, T.G. Langdon, M.J. Zehetbauer, Y.T. Zhu, Mater. Res. Lett. 4 (1) (2016) 1–21.
[2] L.G. Sun, G. Wu, Q. Wang, J. Lu, Mater. Today 38 (2020) 114–135.
[3] A. Rajabzadeh, F. Mompiou, M. Legros, N. Combe, Phys. Rev. Lett. 110 (26) (2013) 265507.
[4] Q. Zhu, G. Cao, J.W. Wang, C. Deng, J.X. Li, Z. Zhang, S.X. Mao, Nat. Commun. 10 (2019) 156.
[5] K.L. Merkle, L.J. Thompson, F. Phillipp, Phys. Rev. Lett. 88 (22) (2002) 225501.
[6] S.E. Babcock, R.W. Balluffi, Acta Metall. 37 (9) (1989) 2367–2376.
[7] S.E. Babcock, R.W. Balluffi, Acta Metall. 37 (9) (1989) 2357–2365.
[8] E.P. George, D. Raabe, R.O. Ritchie, Nat. Rev. Mater. 4 (8) (2019) 515–534.
[9] Y. Zhang, T.T. Zuo, Z. Tang, M.C. Gao, K.A. Dahmen, P.K. Liaw, Z.P. Lu, Prog. Mater. Sci. 61 (2014) 1–93.
[10] Q.Q. Ding, Y. Zhang, X. Chen, X.Q. Fu, D.K. Chen, S.J. Chen, L. Gu, F. Wei, H.B. Bei, Y.F. Gao, M.R. Wen, J.X. Li, Z. Zhang, T. Zhu, R.O. Ritchie, Q. Yu, Nature 574 (7777) (2019) 223–227.
[11] R.P. Zhang, S.T. Zhao, J. Ding, Y. Chong, T. Jia, C. Ophus, M. Asta, R.O. Ritchie, A.M. Minor, Nature 581 (7808) (2020) 283–287.
[12] D. Utt, A. Stukowski, K. Albe, Acta Mater. 186 (2020) 11–19.
[13] T. Yang, Y.L. Zhao, W.P. Li, C.Y. Yu, J.H. Luan, D.Y. Lin, L. Fan, Z.B. Jiao, W.H. Liu, X.J. Liu, J.J. Kai, J.C. Huang, C.T. Liu, Science 369 (6502) (2020) 427–432.
[14] F. Maresca, W.A. Curtin, Acta Mater. 182 (2020) 144–162.
[15] Y.F. Ye, Y.H. Zhang, Q.F. He, Y. Zhuang, S. Wang, S.Q. Shi, A. Hu, J. Fan, Y. Yang, Acta Mater. 150 (2018) 182–194.
[16] D.L. Olmsted, S.M. Foiles, E.A. Holm, Scr. Mater. 57 (12) (2007) 1161–1164.
[17] D.L. Olmsted, S.M. Foiles, E.A. Holm, Acta Mater. 57 (13) (2009) 3694–3703.
[18] Z.L. Pan, T.J. Rupert, Phys. Rev. B 93 (13) (2016) 134113.
[19] Z.L. Pan, T.J. Rupert, Scr. Mater. 130 (2017) 91–95.
[20] D.V. Ragone, Thermodynamics of Materials, JohnWiley & Sons, 1995.
[21] V.A. Ivanov, Y. Mishin, Phys. Rev. B 78 (6) (2008) 064106.
[22] J. Schafer, K. Albe, Acta Mater. 60 (17) (2012) 6076–6085.
[23] M. Legros, D.S. Gianola, K.J. Hemker, Acta Mater.. 56 (14) (2008) 3380–3393.